Passive bistatic radar using DVB-T receivers as general-purpose software-defined radio receivers

Weike Feng,[1] Jean-Michel Friedt,[2, a)] Grigory Cherniak,[1] and Motoyuki Sato[3]

[1)] *Graduate School of Environmental Studies, Tohoku University, Sendai, Japan.*

[2)] *FEMTO-ST, Time & Frequency department, Besançon, France.*

[3)] *Center for Northeast Asian Studies, Tohoku University, Sendai, Japan.*

(Dated: 18 August 2018)

We investigate the use of low-cost digital video broadcast-terrestrial (DVB-T) receivers as general-purpose software-defined radio (SDR) receivers for passive bistatic radar (PBR) applications. Two DVB-T receivers are synchronized using a common clock to perform coherent measurements. By exploiting the direct-path signal in the surveillance channel, we use the cross-correlation process to estimate the time offset between the data streams of reference and surveillance channels caused by the USB communication. We demonstrate the detection of static and moving targets as well as short-range targets, including a landing airplane at 8 km, multiple ships with different velocities, and vehicles within 20 m from the receiver acquiring at a 2 MHz bandwidth, by using Japan's ISDB-T digital TV signal broadcast. We also propose to improve the range resolution of the designed PBR system by combining multiple SDR receivers tuned to different carrier frequencies. The designed system and proposed method can be used for various applications, such as airplane navigation, harbor protection, and traffic density monitoring.

[a)]jean-michel.friedt@femto-st.fr; http://jmfriedt.free.fr/

I. INTRODUCTION

Active radar measurement is associated with high power and broadband emitters. The radar signals from the emitter decay as a function of the product of the square of the source-target distance and the square of the target-receiver distance. Therefore, stronger emission powers are required than that required for one-way communication applications. Moreover, because the radar range resolution is inversely proportional to its bandwidth, broadband signals are required for a high radar range resolution. An alternative to using a dedicated radar emitter is to use some of the radiofrequency signal sources already deployed for various purposes[1–7]: for example, frequency-modulated broadcast emitters, digital audio broadcasting emitters, and digital terrestrial television broadcasting (DTTB) emitters. Use of these sources is advantageous because there is no requirement for frequency allocation for specific applications.

Use of non-cooperative sources for a radar application establishes a passive radar system[8], which is intrinsically bistatic because the transmitter and the receiver are at different locations. Passive bistatic radar (PBR) has been extensively studied for different applications by adopting different sources[9–14]. Although PBR can work independently from the employed waveforms, its performance (measured in terms of parameters such as spatial resolution and ambiguity), coverage area, and available period are mainly determined by the adopted source[15]. Among the different sources, DTTB signals can provide a superior ambiguity function compared to that provided by conventional analog signals, cover an urban-wide area because of the high transmission power, and facilitate continuous measurement. Therefore, DTTB signals are extensively studied for detecting airplanes[16], ships[17], and vehicles[18]. In Japan, Integrated Services Digital Broadcasting Terrestrial (ISDB-T) has been used as the DTTB standard[19]. Some studies of PBR using the ISDB-T signal have been conducted in the last decade[20,21].

Recently, conversion of processing steps from hardware to software has been an ongoing trend, which is driven not only by the flexibility and reconfigurability of software with respect to hardware but also by the lower cost of consumer electronics[22–26]. Communication modems had followed this trend in the 1990s, and now radiofrequency reception peripherals are following a similar trend. Porting the driver of a digital video broadcast-terrestrial (DVB-T) receiver to the Linux operating system led to the discovery that Realtek RTL2832U-based

DVB-T receivers can serve as general-purpose software-defined radio (SDR) receivers, including for the development of high grade scientific instruments[27]. The flexibility of SDR receivers allows for the use of a single affordable hardware in a wide range of fields, including oscillator characterization[28], communication, time transfer[29], or electromagnetic wave propagation conditions. Their broad availability and low cost have made them popular among amateur SDR enthusiasts, including those using the open-source GNU Radio SDR framework[30]: the DVB-T receivers are supported as I/Q coefficient sources with sample rate up to 2.4 Msamples/s and 8-bit resolution, which are suitable for many analog and low-bandwidth digital communication modes, thus making them ideal for adapting to educational material. Since 2010, through the introduction of the now-defunct Elonics E4000 and with the latest versions that use the Rafael Micro R820T2, several radiofrequency frontends have been made available for signal amplification and down-conversion to baseband.

In this study, we use low-cost SDR receivers to illustrate PBR processing techniques to a wide audience. First, we review the fundamentals of passive radar signal processing. Then, a PBR system is designed using DVB-T receivers. We then demonstrate the process of coherent measurements using two DVB-T receivers synchronized by a common clock. Experimental results of mapping stationary and moving targets are presented. Finally, we present the improvement of the range resolution by combining multiple SDR receivers, each tuned to a different carrier frequency. The presented techniques are generally applicable whenever multiple SDR receivers are to be combined either for correlation measurement, bandwidth extension for improved timing resolution or phase measurement with respect to an unknown reference signal in general.

II. FUNDAMENTALS OF PASSIVE RADAR SIGNAL PROCESSING

The underlying requirement for passive radar application is to measure the signal emitted by a non-cooperative source, called the reference signal, and the signal reflected by targets, called the surveillance signal. A cross-correlation technique is required to identify delayed copies of the reference signal in the surveillance signal. As will be illustrated in section IV, in the static case, the cross-correlation technique used is simply the direct cross correlation of surveillance signal $S(t)$ and reference signal $R(t)$ and the output is therefore only dependent upon the time delay τ between these signals:

$$\chi(\tau) = \int_{-\infty}^{+\infty} S(t) \cdot R^*(t-\tau)dt \tag{1}$$

Considering that the Fourier transform of the cross-correlation χ is the product of the Fourier transform of $S(t)$ multiplied by the complex conjugate of the Fourier transform of $R(t)$, Eq. 1 can be effectively calculated by implementing the fast Fourier transform (FFT). The non-cooperative source is not noise but has some structured information that may repeat in time or frequency. Therefore, we must analyse the spectral characteristics of the source to assess its suitability for passive radar application[31].

After demonstrating the static target mapping, we will consider the mapping of moving targets in section V. In the bistatic configuration, a target moving at a velocity v introduces a maximum Doppler shift of $f_D = 2f_0\frac{v}{c}$ on the reflected signal, where f_0 is the carrier frequency and c is the velocity of electromagnetic waves. Therefore, cross-correlation of the surveillance signal $S(t)$ with the reference signal $R(t)$, time-shifted by τ and frequency-shifted by f_D, naturally yields the following cross-ambiguity function:

$$\chi(\tau, f_D) = \int_{-\infty}^{+\infty} S(t) \cdot R^*(t-\tau)\mathrm{e}^{-j2\pi f_D t}dt \tag{2}$$

To reduce the computational complexity, we will use the batch algorithm to calculate Eq. 2 effectively[32]. First, the large dataset is parsed into small batches such that the Doppler shifts of targets within each batch are negligible. For each batch, cross-correlation is performed by implementing FFT. Then, because the direct-path interference and echoes from stationary targets for different batches show small changes, mean-value subtraction is performed to reduce their influences. Finally, the Fourier transform along the batch direction provides the long-term evolution of the Doppler frequencies of the targets.

Ideally, the associated cross-ambiguity function when applying copies of the reference signal as surveillance signals would be a Dirac function. However, in practical application, the sources may exhibit some undesirable properties in the time or frequency domain, which can be erroneously interpreted as detected targets. The ambiguity function of the source obtained by auto-correlating the reference signal with its time-shifted and Doppler-shifted copies provides information on such undesirable property, which can be used to prevent false target detection. The ambiguity functions of various sources have been documented[15]. In Sendai (Japan), three television towers emit 3-kW signals at a frequency range of 470–570

MHz, as shown in Fig. 1. We use the 509-MHz channel for the moving target detection process, and its ambiguity function is given in Fig. 2, in which the information at ±220 Hz offset should not be mistaken for targets. We note that other channels will give the similar results, which are not shown in this paper for concision.

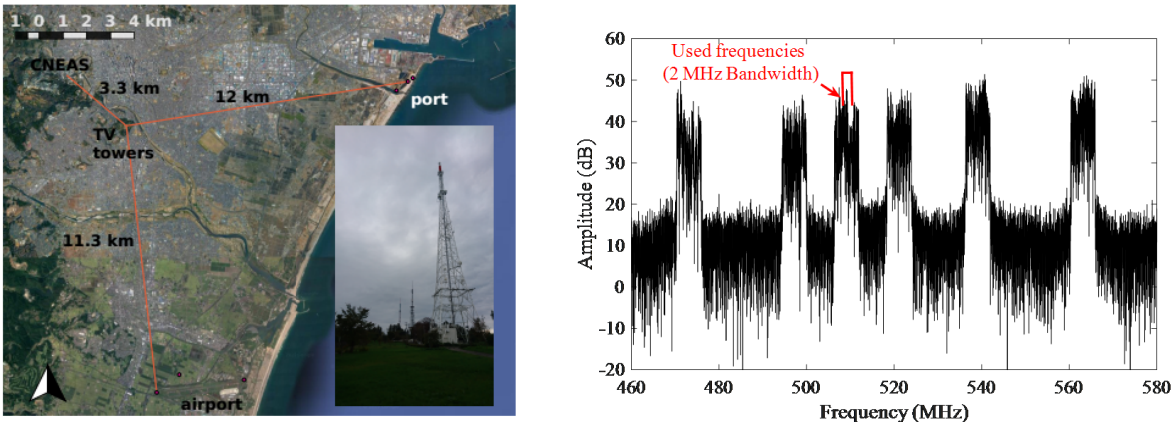

FIG. 1. Left: Three TV towers located 3.3 km from the CNEAS laboratory broadcast in the Sendai (Japan) area. Background map: Google Maps. Right: Spectrum of the six terrestrial digital television stations broadcasting in Sendai.

For short-range applications with a bandwidth of only 2 MHz, because it is unnecessary and impractical to perform range compression, only 1D Fourier transform is used to estimate the Doppler frequency of targets. Therefore, in this case, we apply $\tau = 0$ in Eq. 2, giving:

$$\chi(f_D) = \int_{-\infty}^{+\infty} S(t) \cdot R^*(t) \mathrm{e}^{-j2\pi f_D t} dt \tag{3}$$

This can be effectively calculated by FFT, as will be described in section V. Since we apply $\tau = 0$, it is assumed that the target is limited within the first bistatic range cell, i.e. the short range is defined as 150 m.

III. REQUIREMENT OF COHERENT MEASUREMENTS

Many studies have demonstrated the ability to perform coherent measurements using two DVB-T receivers synchronized by a common clock[33,34]. However, apart from the result description, these studies do not provide a formal and detailed description of the procedure that was followed to acquire the data.

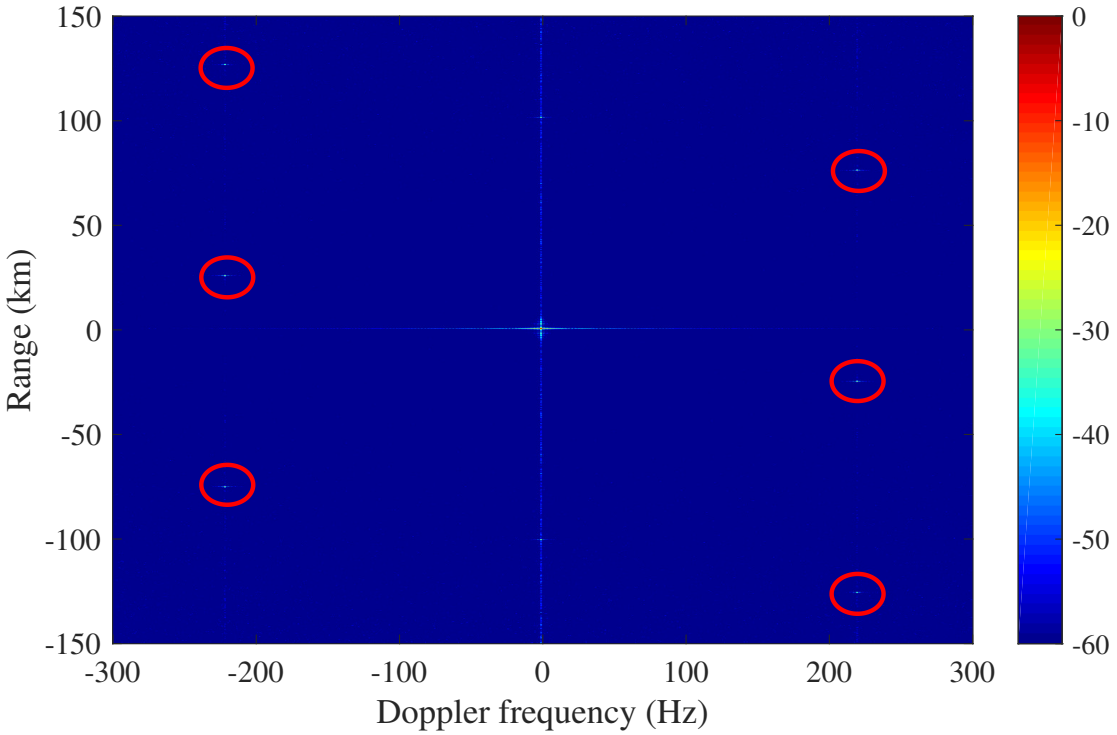

FIG. 2. Ambiguity function of the ISDB-T signal in Sendai, Japan.

Time-delayed copies of the reference signal in the surveillance signal can be identified under the following three conditions: (1) the local oscillator of both radiofrequency receivers must be coherent over the duration of the analysis, (2) the data transferred by the two receivers must be synchronous, and (3) the direct wave reaching the surveillance receiver must not overwhelm the weak reflections from distant targets. These conditions can be achieved by using two consumer electronic DVB-T receivers, with the local oscillator of one receiver used as a clock for the other one, as shown in Fig. 3.

However, in the case of DVB-T receivers used in consumer electronics, to achieve the target carrier frequency, the quartz oscillator is set at a universal serial bus (USB) clock frequency and multiplied by a phase-locked loop (PLL) by the radiofrequency frontend. In coherent measurements, because of the use of the PLL, although fine frequency steps can be achieved by dithering, some phase coherence loss will be introduced. Moreover, the PLL behavior's dependence on temperature introduces a phase difference between the two receivers. The frequency dithering, active as a default configuration of the `librtlsdr` library in the Debian distribution of Linux, as shown in Fig. 4, is deactivated by modifying

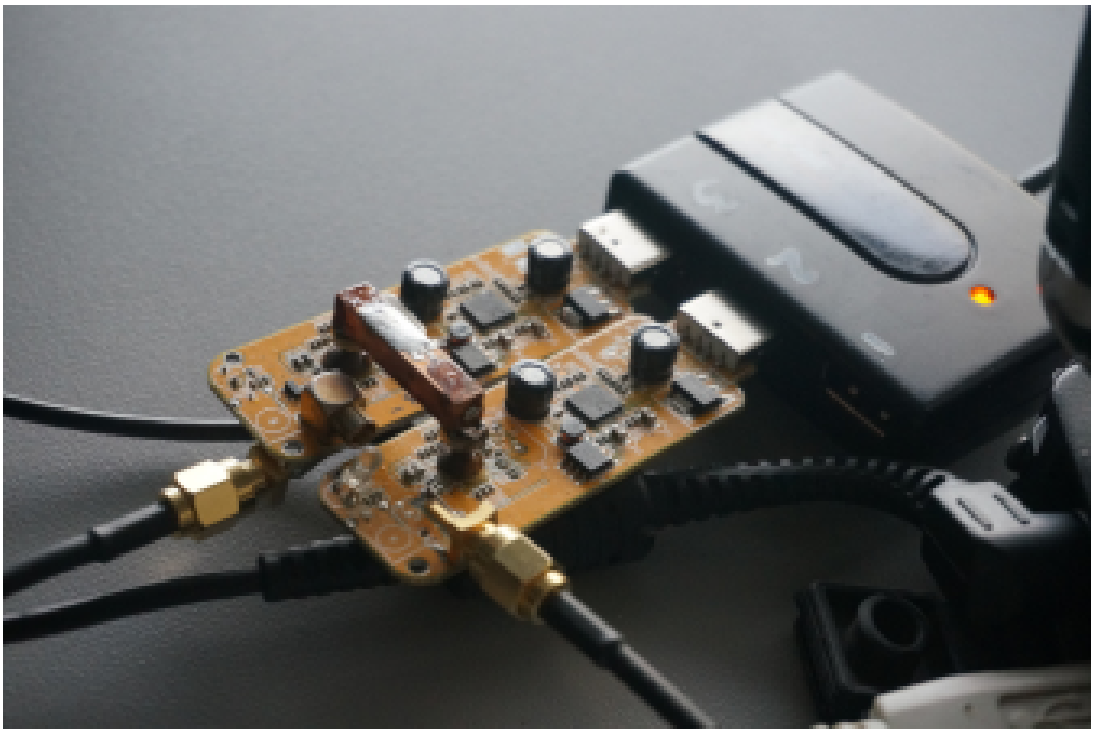

FIG. 3. Experimental setup, where a thermal link made by a copper beam is put between the two radiofrequency frontends. The reference oscillator output from one receiver feeds the clock signal of the other receiver.

the software[35] and compiling a custom version of the `osmosdr` GNU Radio source block linked against the updated library. Temperature drift is tackled by providing a thermal link between the two receiver frontends.

The data transmission synchronization is addressed at the post-processing level. DVB-T receivers communicate over a USB, so the latency between two measurement initialization sequences cannot be predicted. Indeed, the data stream start time is observed to randomly vary as GNU Radio triggers the measurements from both dongles asynchronously. However, once the data stream starts, the time offset is observed to be constant and no sample loss is observed for data rates below 2.048 Msamples/s. The time offset between the two data streams is observed to mostly range within ± 500 μs, or ± 1000 samples when sampling at 2 Msamples/s.Because a strong direct-path interference is always received by the surveillance channel, identifying the time delay by cross-correlating two signals is possible. However, we emphasize that this initial calibration only remains valid as long as the data stream remains

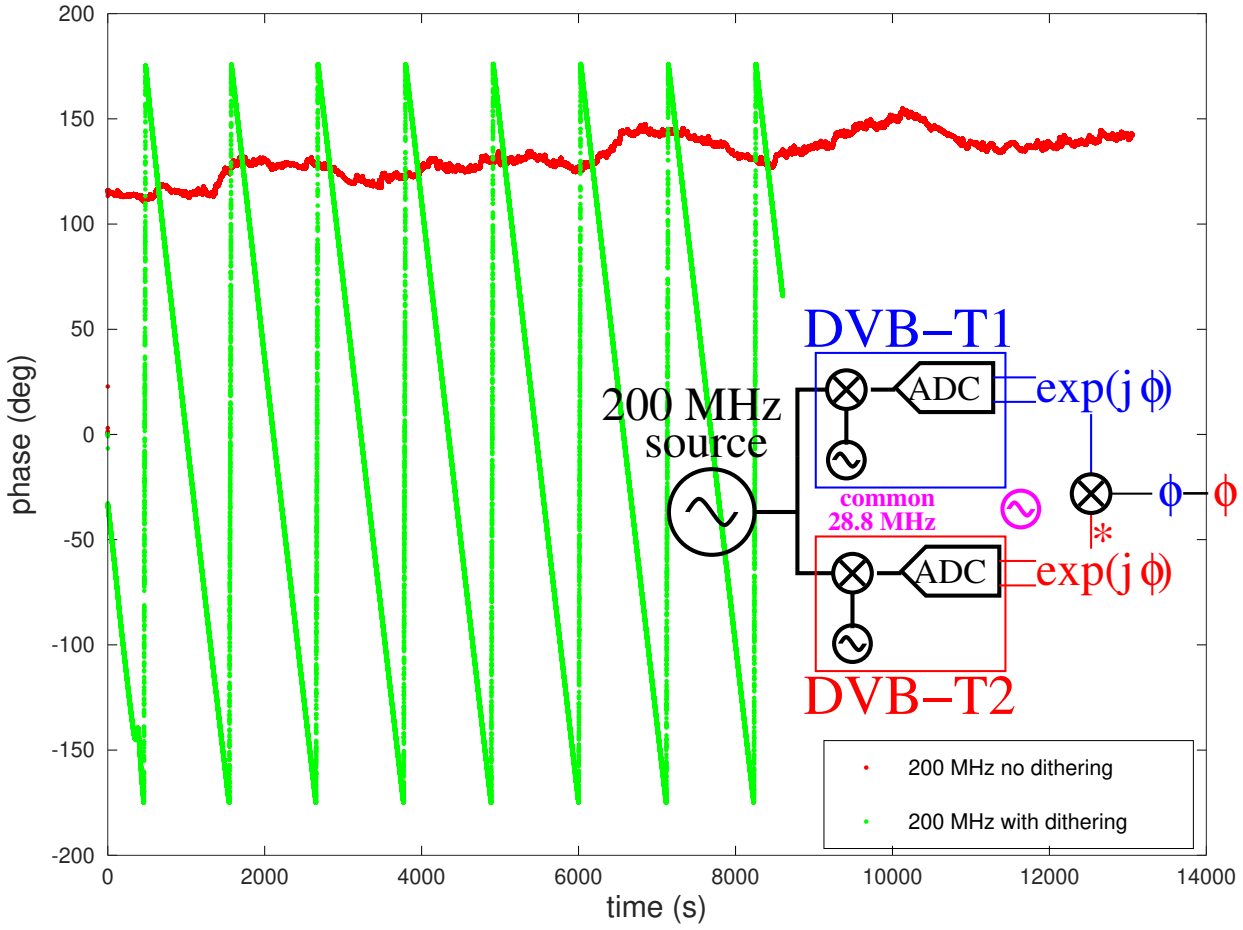

FIG. 4. Impact of dithering (green active, red deactivated) on the phase difference between the outputs of two DVB-T receivers fed by the same oscillator.

uninterrupted.

IV. APPLICATION TO STATIC TARGET DETECTION

Having described the basic setup and processing sequence, we now demonstrate a measurement using the experimental setup described in the previous section. We used a fixed 18-element Yagi-Uda antenna that provides the reference signal and an 18-element surveillance Yagi-Uda antenna that scans over a 170° angular range in azimuth direction incrementally with 5° step. The nominal horizontal and vertical 3 dB beamwidth is $30 \pm 5°$ for such antenna models. For these static targets, the cross-correlation calculation was performed using Eq. 1. GNU Radio is used to achieve a real-time display of the cross-correlation result between two DVB-T receivers as the data are being acquired, which is a key feature with

respect to post-processing to ensure that the collected data are usable in the field.

The real-time cross-correlation was achieved by converting the continuous data stream into vectors, followed by Fourier transform of each vector, computation of the product of one resulting vector and the complex conjugate of the other vector, and finally inverse Fourier transform of the product vector. All these steps are available as processing blocks in GNU Radio and can be readily implemented for real-time analysis.

Figure 5 (top) illustrates the map obtained from the above-mentioned cross-correlation process: the returned signals are maximum in the azimuth of the nearest buildings. However, the poor range resolution associated with the low measurement bandwidth provides a low spatial resolution for such short-range measurements. If the DVB-T receivers are replaced with a radiofrequency-grade oscilloscope , such as an Agilent 54850 sampling at 10 Gsamples/s, and an external amplifier and a down-converter are used, then the resulting map of the signals reflected by the short-range and far-range buildings would be consistent and considerably sharper, as shown in Fig. 5 (bottom). The flexibility of GNU Radio and SDR has been validated by using a digital oscilloscope, as demonstrated by using the signal source we provide at[36], instead of the low-bandwidth DVB-T receivers.

V. APPLICATION TO MOVING TARGET DETECTION

A moving target has the Doppler frequency shift introduced by its motion, which can help to differentiate it from the static clutter. We demonstrate moving target detection on the range-Doppler plane of aircrafts and ships; the former exhibit large velocities even at their landing stage, and the latter exhibit smaller velocities but a larger radar cross-section (RCS).

A. Airplane detection

The experiment was conducted near the Sendai airport, shown in Fig. 1: despite the short range (0–10 km) demonstration, the objective of this experimental framework is to provide a controlled experimental environment with visual assessment of the plane presence, as well as matching the non-cooperative emitter radiation pattern[37] oriented towards the ground rather than the sky, as would be needed for monitoring cruising planes.

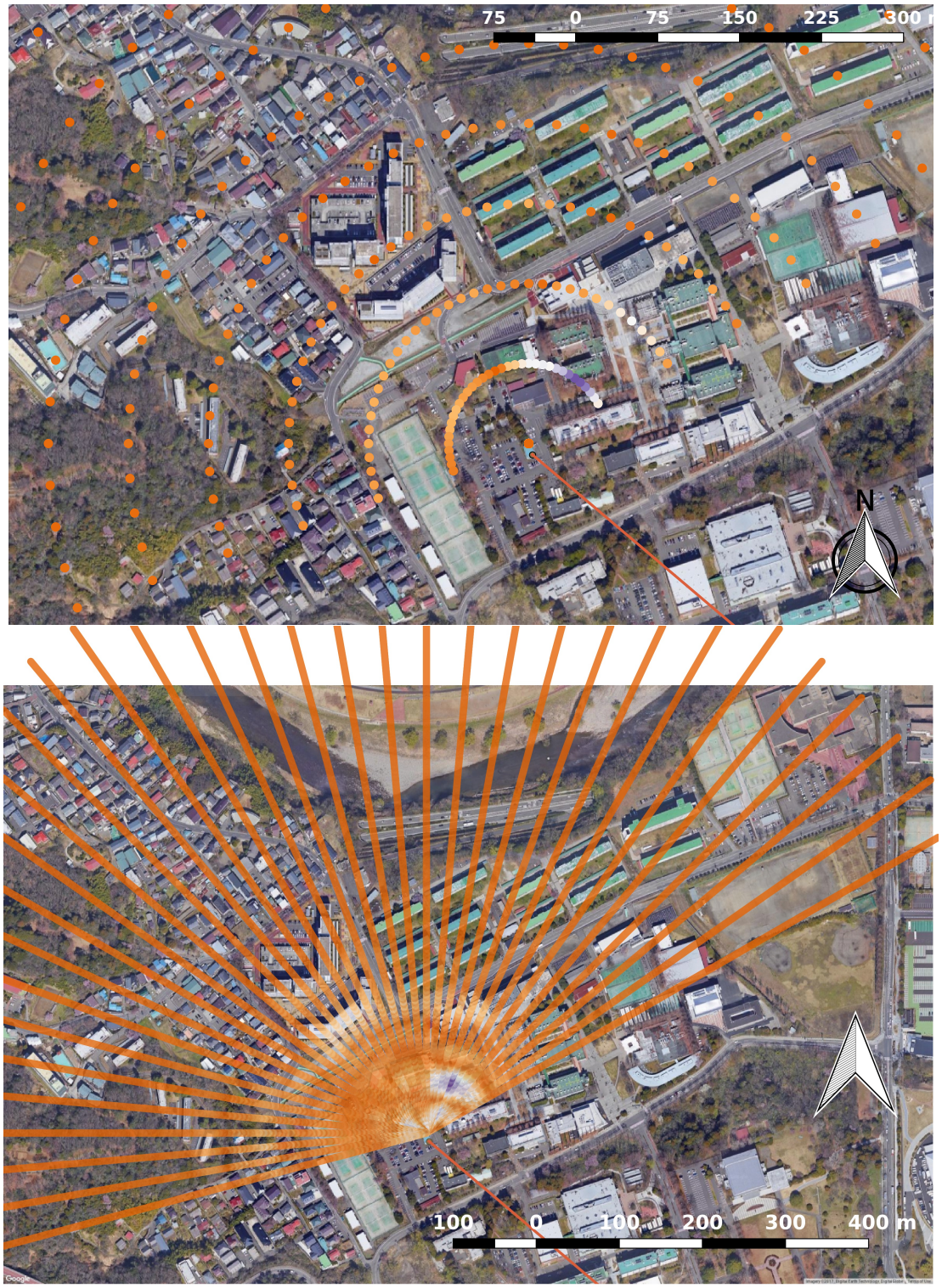

FIG. 5. Cross-correlation result as a function of azimuth and range obtained by (top) DVB-T receivers and (bottom) a radiofrequency-grade oscilloscope.

The acquisition parameters were defined by the characteristics of the target. Since air-

planes were observed in their final stage of landing, we assume a flight velocity of maximum 360 km/h, which introduces a Doppler frequency shift of 333 Hz on the 500 MHz carrier. While a 2-MHz-wide analysis bandwidth only allows for a range resolution of 150 m, an airplane flying at 360 km/h covers 150 m in 1.5 s. Hence, we reach a tradeoff between Doppler frequency resolution and computational complexity by selecting 0.5-s-long data segments, which provide a 2-Hz Doppler frequency resolution, during which the airplane travels a distance of 50 m. As shown in Fig. 6, the airplane is visible far from the clutter at a bistatic range of approximately 8 km. In addition, nearer-range targets, such as the cars moving on the highway, could also be detected, as indicated by the rectangles in Fig. 6: the nature of these near range targets is best assessed on a movie provided as supplementary material[38], in which the velocity is observed to be always in the same range compatible with ±100 km/h and a restricted range as would be expected from cars crossing a bridge in a nearby highway.

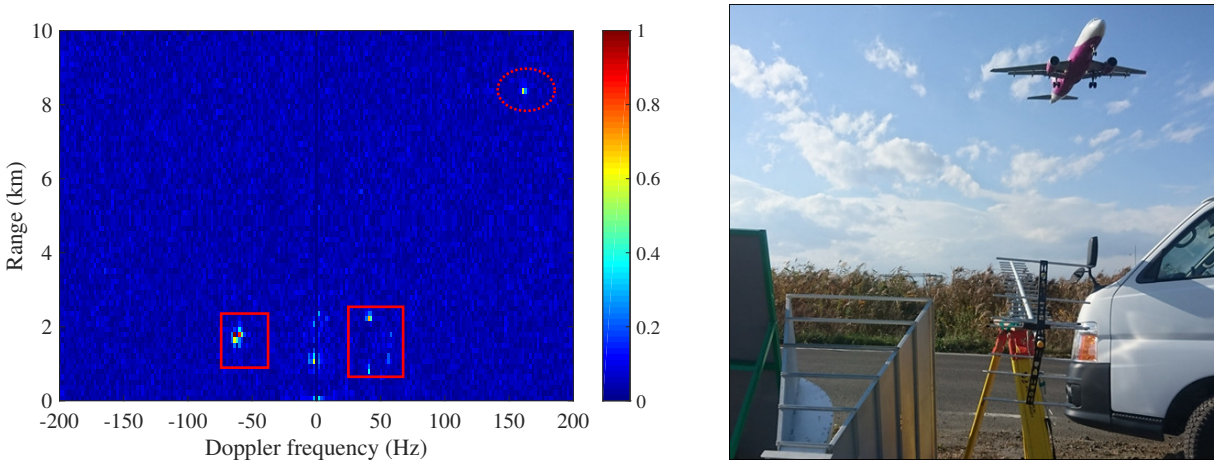

FIG. 6. Range-Doppler map of a landing airplane (left), displayed without mean-value subtraction, and experimental setup (right).

Figure 6 (left) shows the range-Doppler map of a landing airplane when the direct-path interference and echoes from stationary targets were not eliminated by subtracting the mean trace value.

In addition, the range-Doppler map of the airplane when a 125-ms-long integration time is selected, which provides an 8-Hz Doppler resolution, is shown in Fig. 7. By comparing Fig. 7 and Fig. 6, we note that by increasing the integration time to 0.5 s, although the computation time is increased, sidelobes are reduced and the signal-to-noise ratio is significantly improved. Near-range moving cars are well visible above the clutter and the

airplane is identified easily at a far range.

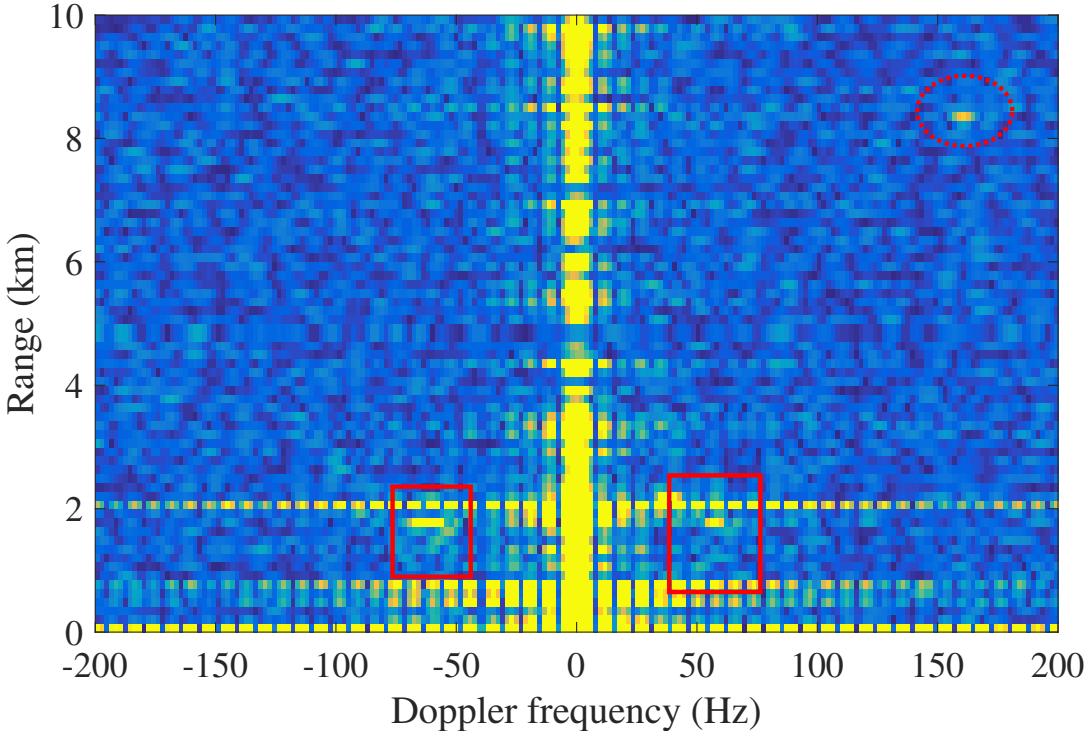

FIG. 7. Range-Doppler map of a landing airplane with a 125-ms integration time.

Various types of airplanes, including large commercial aircraft, smaller two-seater training aircrafts, and helicopters, have been detected in the same day using this system[38]. The measurement sequence durations are limited by the data bandwidth: with 2 Msamples/s, 4 bytes/sample, two channels, and I/Q coefficients, the data rate is 32 MB/s or 1.92 GB/min. Therefore, because of storage limitations, all measurements were maximum 4-minute long. For the identification of the range and velocity analysis during airplane landing, the range-Doppler maps are stacked to obtain a complete trajectory estimation of the airplane. The result for a 1.5 minute long record is illustrated in Fig. 8, where the landing route can be clearly observed, as indicated by the rectangle.

B. Ship detection

Ships entering and leaving the port of Sendai, shown in Fig. 9, were also observed using the designed passive radar. The parameters used here were different from those of the

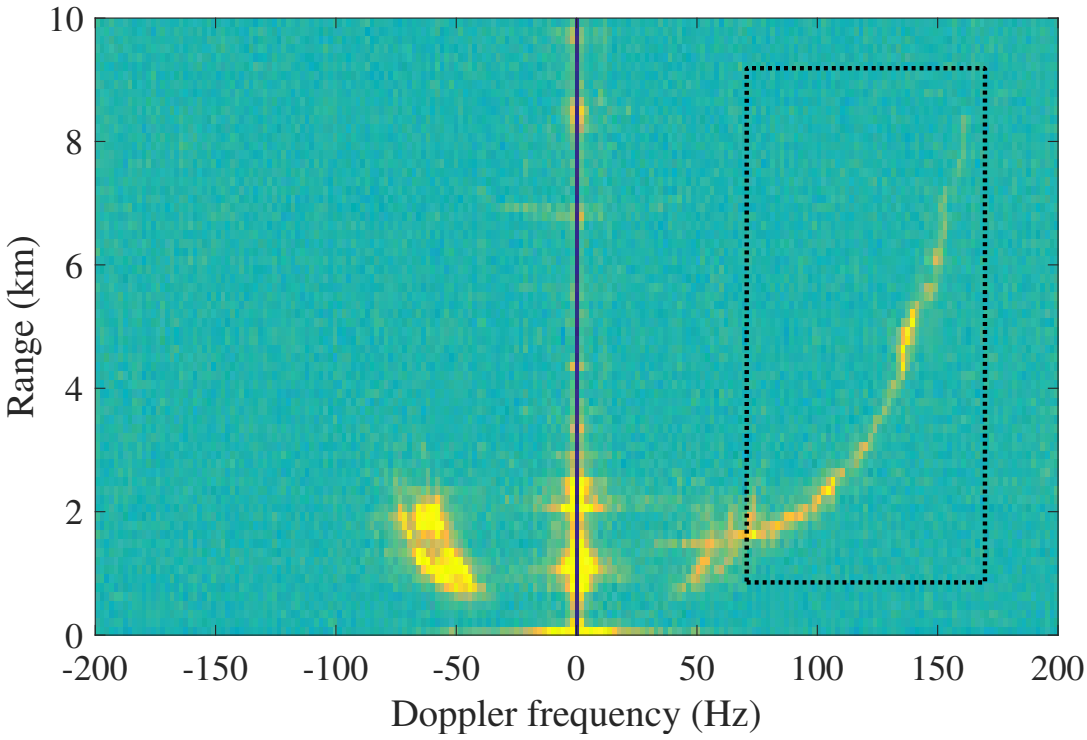

FIG. 8. Trajectory of a landing airplane for a 1.5-minute record.

experiments with the airplanes. Since the ships move much more slowly than airplanes, 2-s-long data segments are selected, which provides a 0.5-Hz Doppler frequency resolution and high signal-to-noise ratio. Fig. 9 and Fig. 10 show the detection and trajectory estimation results for three ships that are visible on the horizon. Two of the ships were moving in opposite directions with respect to the antennas, while the third one was static during the entire measurement duration.

Because ships move slower than airplanes, a strategy was devised to extend the acquisition duration of GNU Radio. Although GNU Radio processes floating point numbers, the DVB-T receivers only sample 8-bit data. Hence, the complex values provided to GNU Radio, ranging from -1 to +1, are scaled by 127 and stored as interleaved 8-bit integers. Therefore, the acquisition duration is increased by 4 times, which results in a record duration of 12 min.

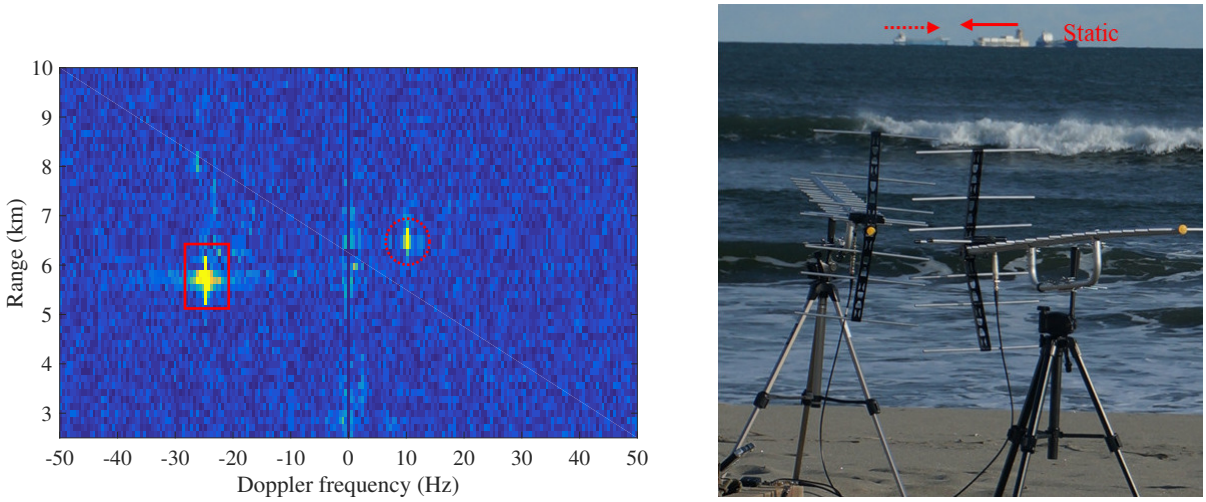

FIG. 9. Range-Doppler map of multiple ships (left), and experimental setup (right).

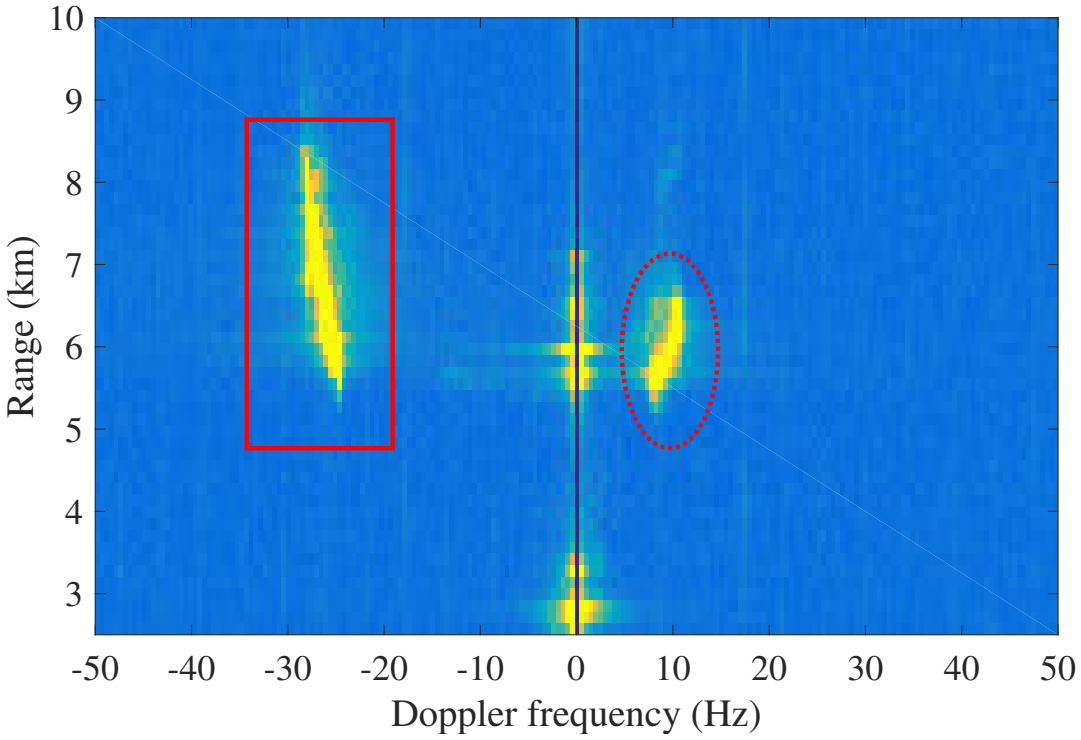

FIG. 10. Ship trajectory estimation result for a 2.7-minute record.

C. Short-range moving vehicles

Finally, we applied PBR measurements using low-cost DVB-T receivers to near-range moving target detection. Since the 2-MHz bandwidth receivers allow for a bistatic range

resolution of only 150 m, the range measurement of a low-RCS target at short range, such as cars or motorbikes, is not feasible. Therefore, we set $\tau = 0$ at a fixed value to calculate the cross-ambiguity function Eq. 2, such that the short-range target detection problem becomes a simple Doppler identification through the Fourier transform, as given in Eq. 3.

Figure 11 shows the result of a 3-minute long dataset analysis, with a 0.5-s integration time. In this measurement case, various vehicles drove toward or away from the surveillance antenna, which induced positive or negative Doppler frequencies (Y-axis), respectively.

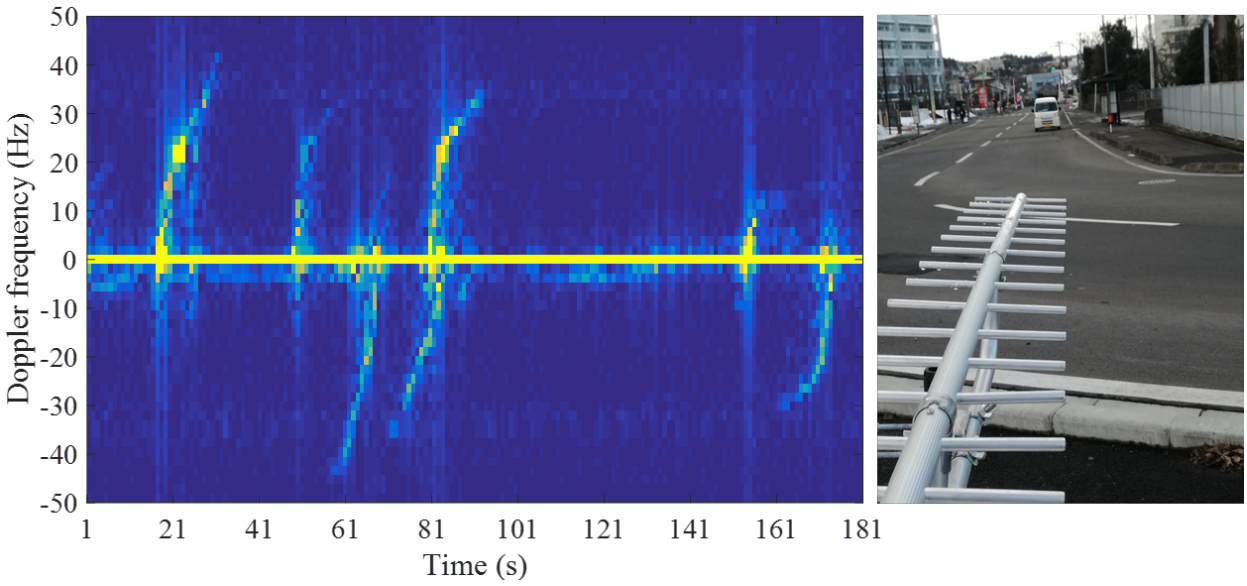

FIG. 11. Doppler evolution (Y-axis) of targets as a function of time (X-axis) for vehicle measurement 1.

Figure 12 shows results of the analysis of another dataset. While acquiring the data, a movie of the road was recorded, from which images were extracted at one frame per second. The images were then manually selected by deleting those without any moving target. This yielded a selection of buses, cars, and motorbikes that drove past the surveillance antenna during the 3-minute long record. Each white line on the bottom of the chart in Fig. 12 is associated with one vehicle. The first vehicle in Fig. 12 is a motorbike: the designed system is efficient enough to allow detection of such a low-RCS target. Here, again, the observed Doppler shift is coherent with vehicles moving at a speed of 30 km/h, and the Doppler shift sign varied depending on whether the target was driving toward or away from the surveillance antenna. All non-zero Doppler traces are associated with a vehicle, and all vehicles in the movie are associated with a radar trace. Hence, the two measurement techniques appear

complementary; the radar measurement provided a quantitative measurement of the vehicle speed and the images provided qualitative information of the presence of the target.

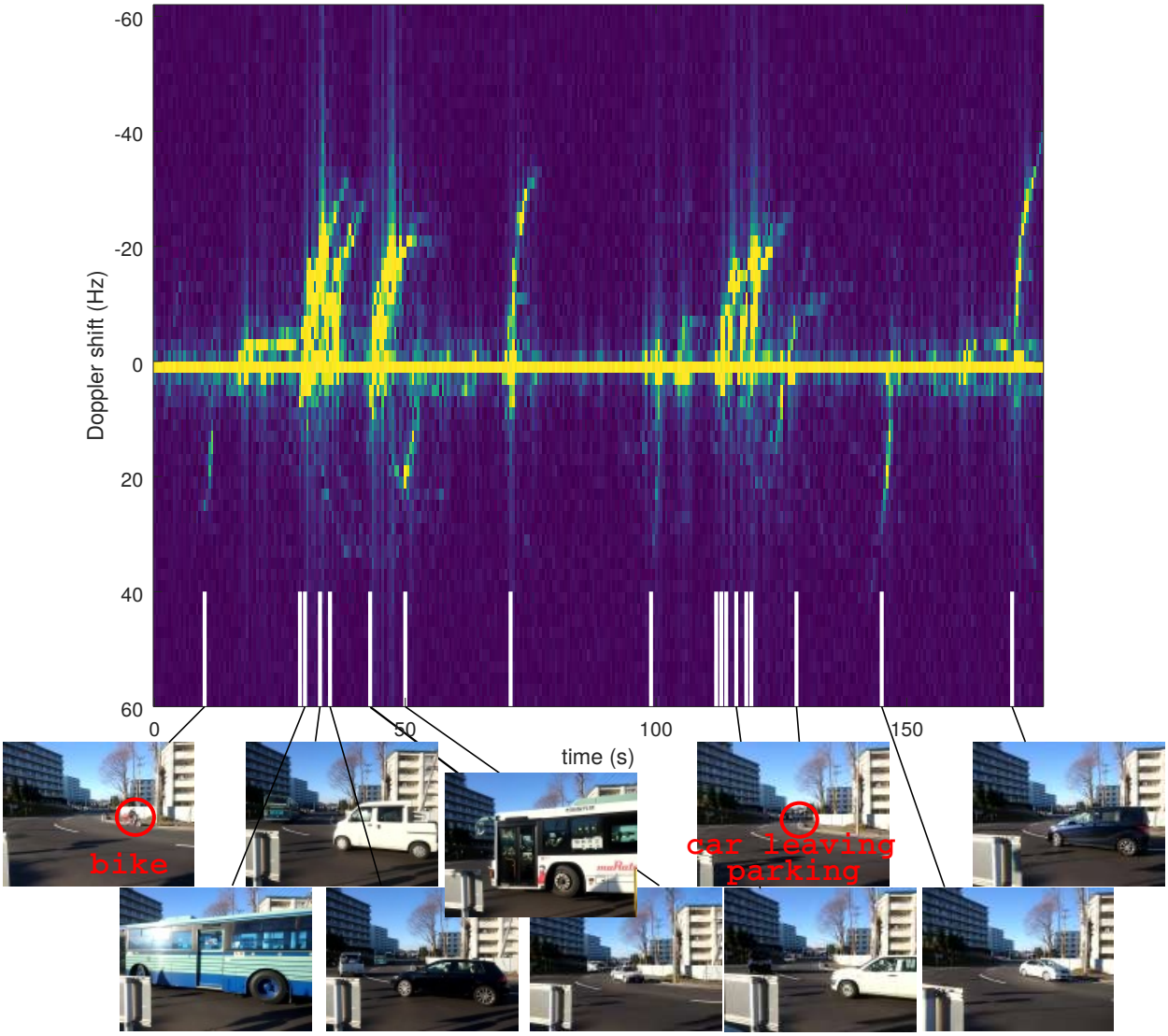

FIG. 12. Top: Doppler evolution (Y-axis) of targets as a function of time (X-axis) for vehicle measurement 2. Bottom: selection of a few images from a movie recorded while acquiring radar data, indicating each time a vehicle is visible in front of the receiver.

VI. RANGE RESOLUTION IMPROVEMENT BY EXTENDING THE NUMBER OF RECORDING CHANNELS

The bistatic range resolution is given by the inverse of the measurement bandwidth. The television channels' bandwidth is as wide as 6 MHz, but each DVB-T receiver can

only sample up to 2 Msamples/s or a range resolution of 150 m. The range resolution can be improved by expanding the measurement bandwidth, which is possible with SDRs, by multiplying the number of receivers, each tuned to a different carrier frequency. Within one given television channel broadcast, two adjacent frequencies allow for sampling up to 4 Msamples/s, thereby halving the range resolution. Furthermore, the flexibility of SDR allows for tuning to different television channels that are characterized by widely different carrier frequencies emitted from the same location, as shown in Fig. 13. In this case, the range resolution is significantly increased but at the cost of high-level sidelobes introduced by the frequency gap between the two sampled datasets[39,40].

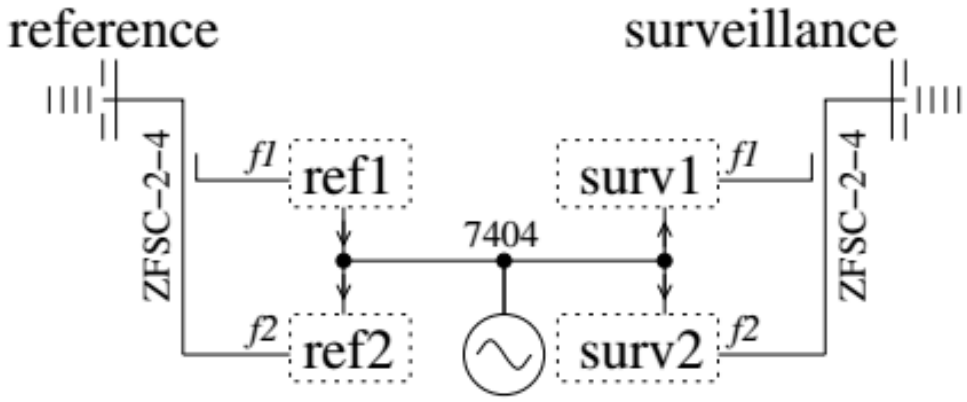

FIG. 13. A passive radar setup with four receivers, with two receivers tuned to different carrier frequencies connected to the reference antenna, while the other two tuned to the same carrier frequency set connected to the surveillance antenna. A single master clock cannot be directly distributed to the three slaves by connecting the oscillator output to the three inputs: a hex-inverted 7404 is used as a buffer between the output and two of the inputs. The MiniCircuits ZFSC-2-4 splitters are used between the antennas and the DVB-T receivers.

In a quad-receiver setup, for the coherent analysis of the signals recorded by two DVB-T pairs tuned to different carrier frequencies, the synchronization procedure for compensating for the delay introduced by the USB communication must be accurate such that the cells in the range-Doppler map are matched. Since the resulting range resolution is increased with respect to the single-channel analysis, interpolation is needed to accurately position the cells in the range direction: any delay between the data recorded by the surveillance and

reference channels, caused by the USB communication, will be observed as a range error, and signals from two sets of reference and surveillance channels will not accumulate coherently to increase the range resolution. Indeed, since multiple channel signals are combined by summing complex spectra obtained after frequency transposition, accurate alignement of the datastreams collected from receivers is mandatory for phase coherence. A two step process is used: initially, samples collected by reference and surveillance channels tuned to the same band are aligned by correlation as described previously, and then digital communication delays between receivers are computed and compensated for with sub-sampling period accuracy using interpolation, assuming that the propagation delay is the same for all channels as expected from a non-dispersive medium as air. Thus improved range resolution is achieved thanks to the increased bandwidth by reaching higher timing resolution than the sampling period as needed to provide phase coherence throughout the spectrum range.

Thus, we analyze the fine synchronization by using the direct wave signals received by both reference and surveillance channels at two different frequencies. Using an oversampling approach, for example by zero-padding the Fourier transform and computing the low-pass filtered inverse Fourier transform, under the assumption that the direct wave is characterized by a single correlation peak, the cross-correlation peak position will provide a time delay with an accuracy better than the sampling rate. By using this time delay on both channel pairs, the targets are positioned in the same range cell, thereby resulting in the range resolution improvement. The acquisition and processing algorithm is summarized as follows:

1. collect data from four SDR receivers, two of which are connected to the reference antenna, while two are connected to the surveillance antenna. The first and third receivers are tuned to one frequency, the second and fourth are tuned to a frequency farther from the first one by more than the sampling bandwidth;

2. synchronize the first two and last two data streams by oversampling the data and selecting the maximum of their cross-correlations;

3. throughout the data analysis, assume the delays introduced by the USB communication latencies to be constant and the stream to be continuous, and shift the oversampled datasets by the delays identified from step 2;

4. combine the synchronized oversampled datasets from the two frequency ranges during

the cross-correlation computation to increase the range resolution. The approach to combine two frequency ranges is given as follows:

(a) assuming that the synchronized oversampled datasets with two carrier frequencies f_1 and $f_2(t)$ are $R_1(t)$, $R_2(t)$, $S_1(t)$ and $S_2(t)$, based on Eq. 1, compute the cross-correlation for each dataset by implementing FFT, giving

$$\chi_1(\tau) = \int_{-\infty}^{+\infty} S_1(t) \cdot R_1^*(t-\tau)dt \tag{4}$$

and

$$\chi_2(\tau) = \int_{-\infty}^{+\infty} S_2(t) \cdot R_2^*(t-\tau)dt \tag{5}$$

(b) combine the cross-correlation results by

$$\chi(\tau) = \chi_1(\tau)\mathrm{e}^{j2\pi f_1\tau} + \chi_2(\tau)\mathrm{e}^{j2\pi f_2\tau} \tag{6}$$

The need for interpolating data through oversampling during the delay matching search is illustrated in Fig. 14. If no oversampling is performed, the datasets collected at each frequency are aligned to within one sampling period, and the cross-correlation peaks of samples collected at both frequencies are not properly aligned to sharpen the correlation peak through destructive interference of the sidelobes. By contrast, upon oversampling, the broadband cross-correlation peak is observed to narrow to one-half of the narrowband width. These measurements were collected by letting both measurement and surveillance channels connect to the reference antenna that points toward the non-cooperative emitter.

In the dataset used to obtain the results shown in Fig. 14, two 2 MHz adjacent frequency bands separated by 2 MHz, namely, 472 $\pm$1 MHz and 474 $\pm$1 MHz, were collected. Combining the two datasets halves the cross-correlation width. Since multiple television channels are broadcast from the same television tower, combining signals emitted from the same location but at widely different frequencies will increase the bandwidth and hence the range resolution. However, the discontinuous frequency acquisitions, with only 2 MHz wide ranges sampled at carrier frequencies differing by several tens of MHz, introduces high sidelobe levels; this makes target identification challenging, as shown in Fig. 15.

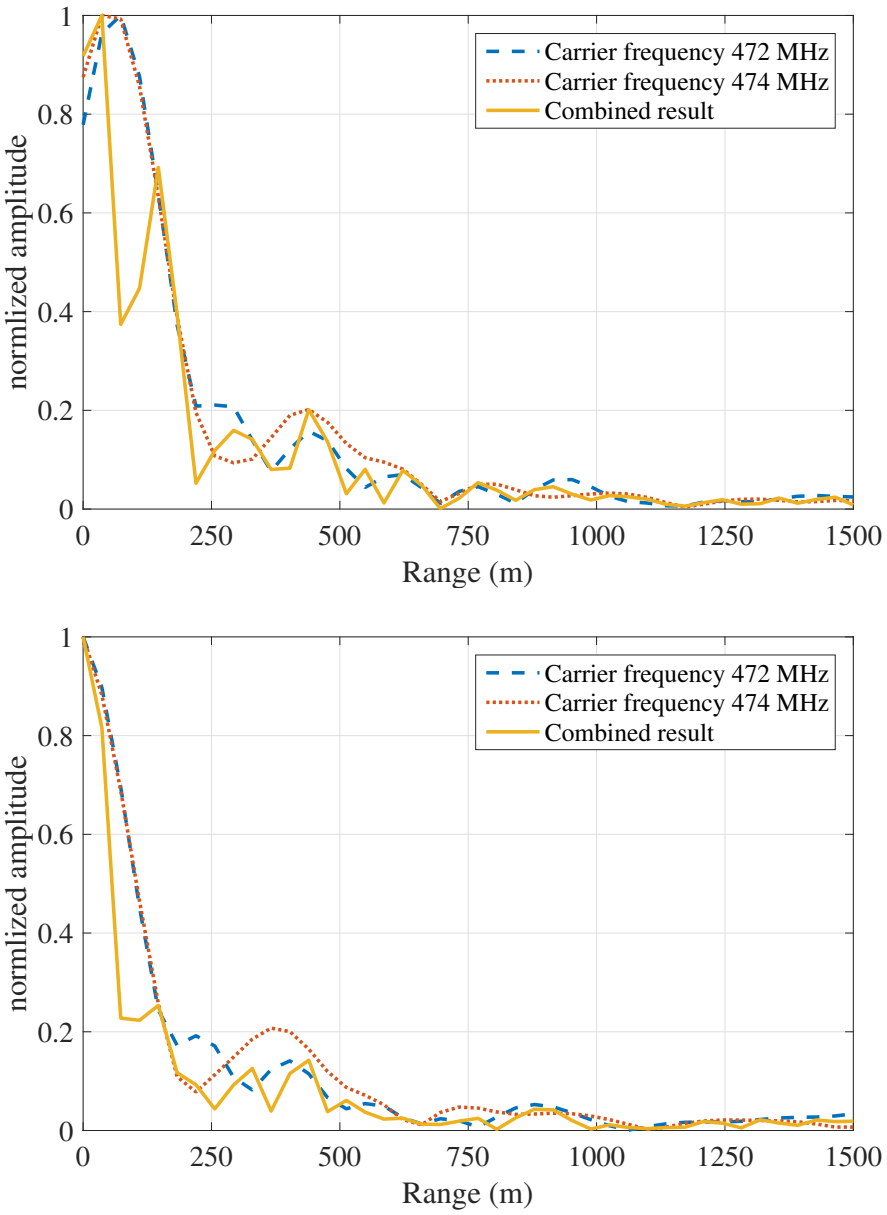

FIG. 14. Cross-correlation results obtained by combining two adjacent frequency bands (top) without interpolation and (bottom) with interpolation. Interpolation allows for aligning both datasets with a resolution beyond one sampling period, hence aligning the cross-correlation peak for improved range resolution.

To further validate the range resolution improvement by combining multiple frequency bands, a field experiment to detect ships was carried out in the Shiogama port near Sendai (Japan) (Fig. 16 (left-top)). The range-Doppler maps of ships obtained by the batch

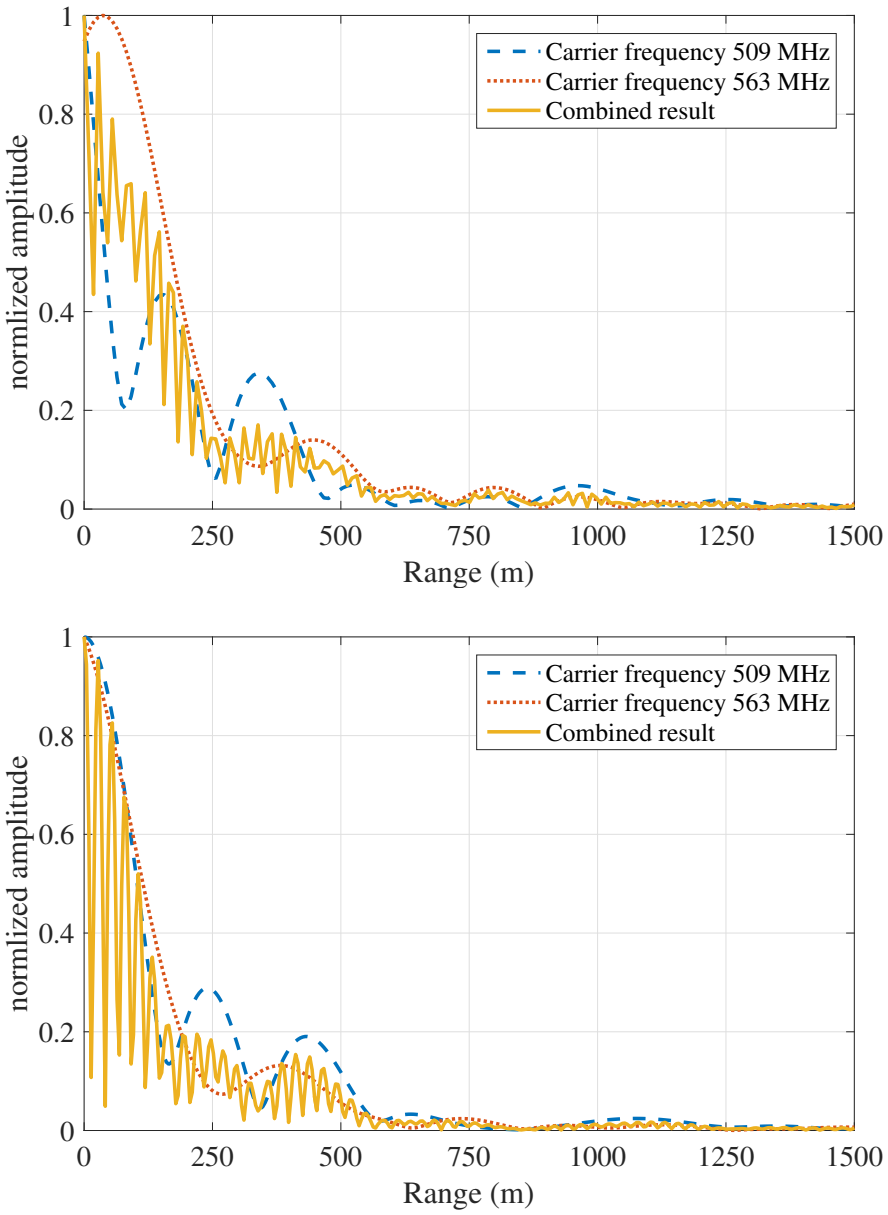

FIG. 15. Cross-correlation results obtained by combining two discontinuous frequency bands (top) without interpolation and (bottom) with interpolation. Due to the frequency gap between the two used frequency bands, high-level sidelobes are produced.

algorithm are shown in Fig. 16, where the right-most ship shown in Fig. 16 (left-top), which has a low-RCS and is the farthest from the receiver setup, is not visible. It can be learned from Fig. 16 (right-top) and (left-bottom) that, both pairs of DVB-T receivers can achieve the range-Doppler map of ships with similar resolution. In addition, the targets are

positioned in the same range-Doppler cells in Fig. 16 (right-top) and (left-bottom). Fig. 16 (right-bottom) shows that, by combining two adjacent frequency bands, the range resolution of the detected ship is increased.

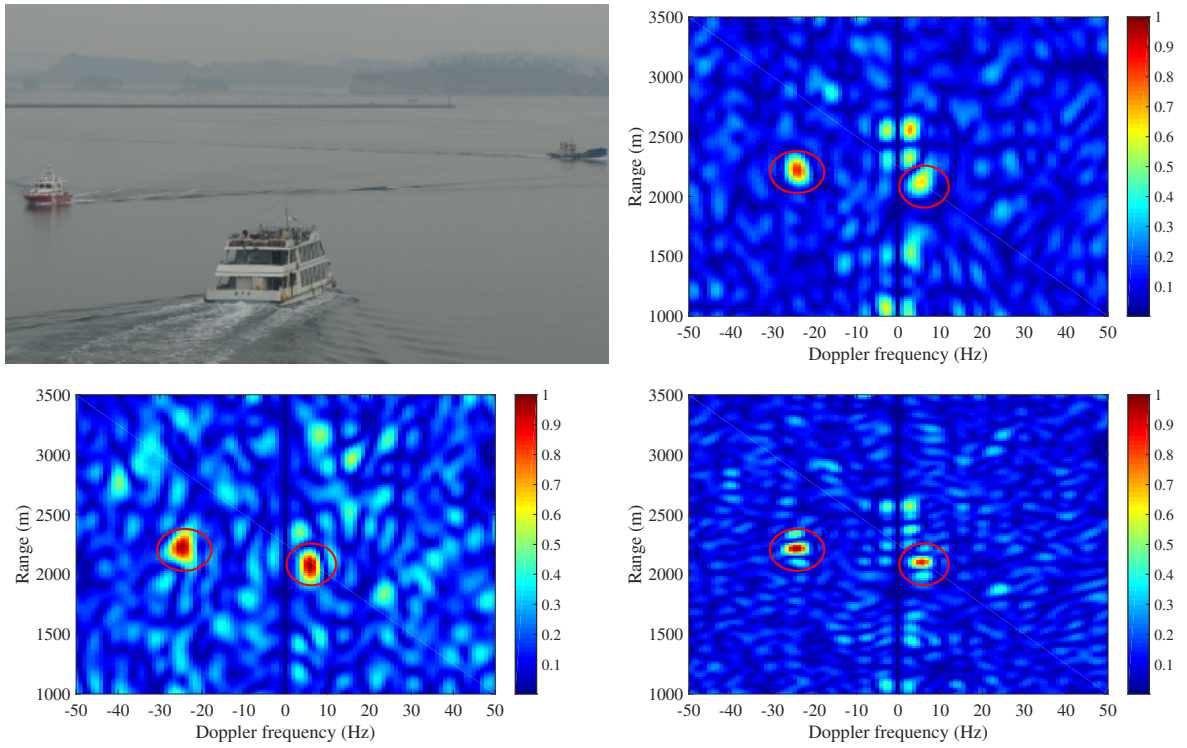

FIG. 16. (Left-top) Ship detection experiment. The range-Doppler maps obtained at a carrier frequency of (right-top) 508 MHz and (left-bottom) 510 MHz, and the range-Doppler map obtained by (right-bottom) combining the two frequency bands, which increases the measurement bandwidth and hence improves the range resolution.

To make the comparison clearer, the cross sections along the range-Doppler position of a target are extracted from Fig. 16, giving Fig. 17. Fig. 17 (top) shows that the range-resolution is improved by combining two frequency bands together, while Fig. 17 (bottom) shows that the Doppler resolution is not influenced by the combination of different channels because the total integration time is unchanged.

VII. CONCLUSION

In this study, we demonstrate the use of consumer-grade DVB-T receivers as general-purpose SDR receivers in PBR detection. We present the processing steps required to

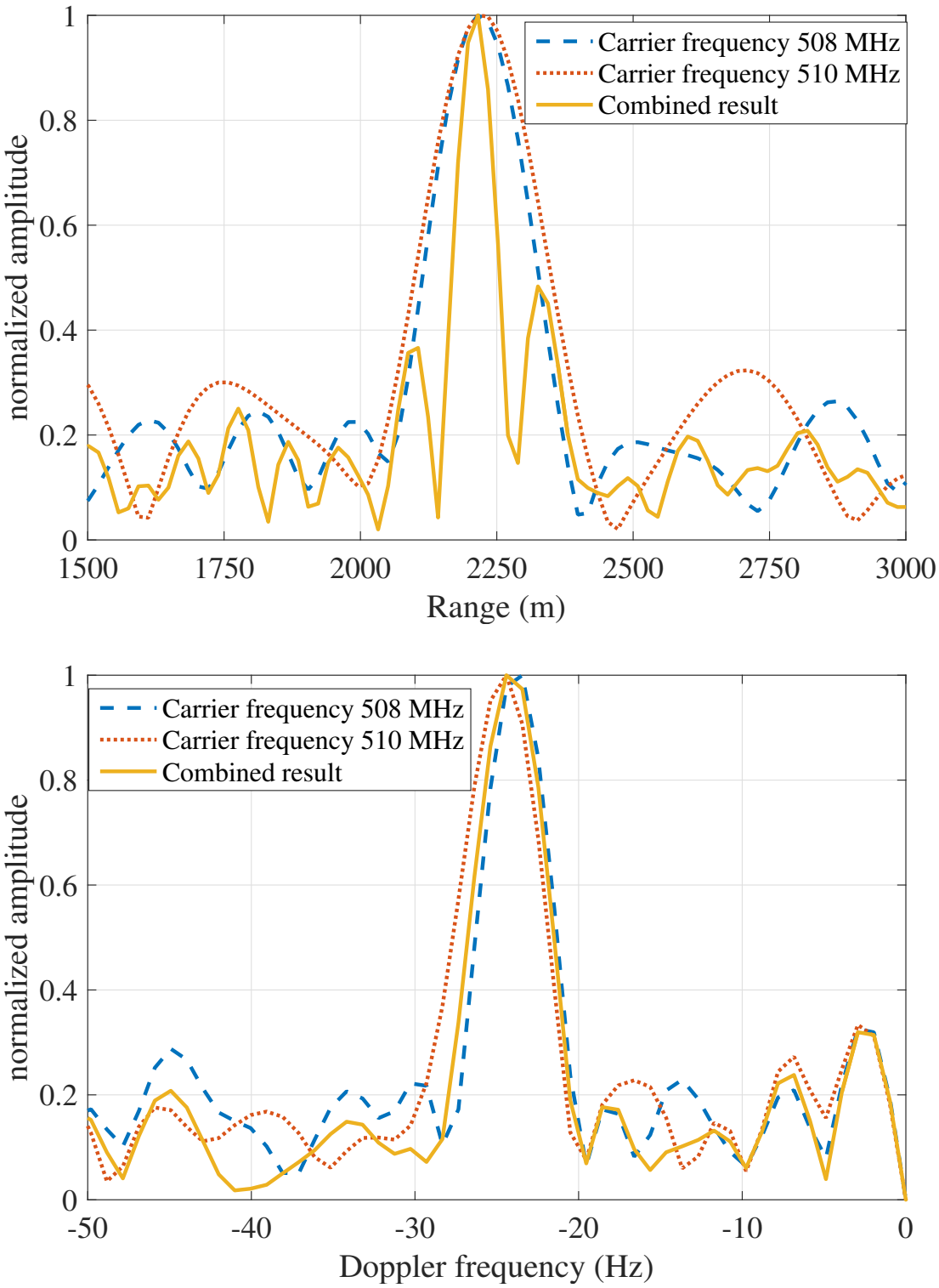

FIG. 17. (Top) Cross-sections along the range direction at a fixed Doppler shift -24.4 Hz, and (bottom) Doppler-frequency cross-sections at a fixed range of 2215 m.

develop the experimental setup, namely, feeding the reference and surveillance receivers with a common clock and tuning the PLL such that dithering is disabled. The time offset between the two data streams remains constant and is calibrated in the post-processing step because the delay introduced by the USB digital communication bus is not deterministic and varies between experiments. No sample loss was observed for sampling rates lower than 2.048 Msamples/s. Despite the low range resolution of such a low bandwidth, various static and moving targets were detected at both far and short ranges. The designed system and proposed method allow detection of airplanes at a far range or cars at a short, undetermined range. Furthermore, simultaneous acquisition of multiple frequency bands, which increases the frequency bandwidth, is demonstrated to improve the range resolution after synchronizing the data streams with a sub-sampling period accuracy.

To improve target identification with range, velocity, and azimuth identification, the proposed setup can be extended to include more surveillance antennas, allowing better azimuth detection. In another work, we propose a novel algorithm for high-resolution and real-time range-Doppler map generation for moving targets[26] by exploiting the sparsity of moving targets and combining the batch algorithm and the advanced compressive sensing algorithm. This technique is expected to further improve the target detection and trajectory estimation performance of the low-cost DVB-T receiver-based PBR system.

ACKNOWLEDGMENTS

This work is supported by JSPS Grant-in-Aid for Scientific Research (A) 26249058. J.-MF is grateful to Tohoku University for granting a position as a three-month visiting scientist to the Center for Northeast Asian Studies (CNEAS). The DVB-T passive radar investigation is partly supported by the French Centre National de la Recherche Scientifique (CNRS) PEPS grant.

REFERENCES

[1]P. E. Howland, D. Maksimiuk, and G. Reitsma, IEE Proceedings-Radar, Sonar and Navigation **152**, 107 (2005).

[2]C. Coleman and H. Yardley, IET Radar, Sonar & Navigation **2**, 366 (2008).

[3]M. Antoniou, Z. Zeng, L. Feifeng, and M. Cherniakov, IEEE Geoscience and Remote Sensing Letters **9**, 477 (2012).

[4]L. Daniel, S. Hristov, X. Lyu, A. G. Stove, M. Cherniakov, and M. Gashinova, IEEE Transactions on Aerospace and Electronic Systems **53**, 3115 (2017).

[5]F. Colone, P. Falcone, C. Bongioanni, and P. Lombardo, IEEE Transactions on Aerospace and Electronic Systems **48**, 1061 (2012).

[6]D. Olivadese, M. Martorella, E. Giusti, D. Petri, and F. Berizzi, in *Synthetic Aperture Radar, 2012. EUSAR. 9th European Conference on* (VDE, 2012) pp. 287–290.

[7]L. Zheng and X. Wang, IEEE Transactions on Signal Processing **65**, 2197 (2017).

[8]H. D. Griffiths and C. J. Baker, *An Introduction to Passive Radar* (Artech House, 2017).

[9]M. K. Baczyk, P. Samczynski, P. Krysik, and K. Kulpa, IEEE Aerospace and Electronic Systems Magazine **32**, 14 (2017).

[10]A. Capria, E. Giusti, C. Moscardini, M. Conti, D. Petri, M. Martorella, and F. Berizzi, IEEE Aerospace and Electronic Systems Magazine **32**, 30 (2017).

[11]J. R. G. Del Arroyo and J. A. Jackson, IEEE Transactions on Aerospace and Electronic Systems **49**, 945 (2013).

[12]P.-O. Frölind, in *Radar Conference (RadarConf), 2016 IEEE* (IEEE, 2016) pp. 1–4.

[13]M.-P. Jarabo-Amores, J.-L. Bárcena-Humanes, P. Gómez-del Hoyo, N. Rey-Maestre, D. Juara-Casero, F.-J. Gaitán-Cabañas, and D. Mata-Moya, IET Radar, Sonar & Navigation **11**, 133 (2016).

[14]D. Gromek, K. Kulpa, and P. Samczyński, IEEE Geoscience and Remote Sensing Letters **13**, 1124 (2016).

[15]A. Evers and J. A. Jackson, IEEE Transactions on Aerospace and Electronic Systems **51**, 3440 (2015).

[16]M. Baczyk, P. Samczynski, and K. Kulpa, in *Radar Conference, 2014 IEEE* (IEEE, 2014) pp. 0502–0506.

[17]A. Capria, M. Conti, D. Petri, M. Martorella, F. Berizzi, E. Dalle Mese, R. Soleti, and V. Carulli, in *IEEE Gold Remote Sensing Conference* (2010).

[18]A. Capria, D. Petri, M. Martorella, M. Conti, E. DalleMese, and F. Berizzi, in *Geoscience and Remote Sensing Symposium (IGARSS), 2010 IEEE International* (IEEE, 2010) pp. 3917–3920.

[19]M. Takada and M. Saito, Proceedings of the IEEE **94**, 251 (2006).

[20]J. Honda and T. Otsuyama, IEEE Antennas and Wireless Propagation Letters **15**, 1787 (2016).

[21]S. Nakamura, K. Suwa, S. Morita, K. Yamamoto, T. Wakayama, T. Oshima, R. Maekawa, and S. Matsuda, in *Geoscience and Remote Sensing Symposium (IGARSS), 2011 IEEE International* (IEEE, 2011) pp. 2837–2840.

[22]P. Mahnke, Review of Scientific Instruments **89**, 013113 (2018).

[23]F. Berizzi, M. Martorella, D. Petri, M. Conti, and A. Capria, in *Radar Conference, 2010 IEEE* (IEEE, 2010) pp. 225–229.

[24]J. Marimuthu, K. S. Bialkowski, and A. M. Abbosh, IEEE Transactions on Microwave Theory and Techniques **64**, 643 (2016).

[25]B. Tuysuz, J. Urbina, and F. Lind, Radio science **48**, 416 (2013).

[26]W. Feng, J.-M. Friedt, G. Cherniak, and M. Sato, IEEE Transactions on Aerospace and Electronic Systems (2018), under review.

[27]T. Nieminen, P. Lähteenmäki, Z. Tan, D. Cox, and P. J. Hakonen, Review of Scientific Instruments **87**, 114706 (2016).

[28]J. A. Sherman and R. Jördens, Review of Scientific Instruments **87**, 054711 (2016).

[29]C. Andrich, A. Ihlow, J. Bauer, N. Beuster, and G. Del Galdo, IEEE Transactions on Instrumentation and Measurement (2018).

[30]T. W. Rondeau, Opportunistic Spectrum Sharing and White Space Access: The Practical Reality , 25 (2015).

[31]H. A. Harms, L. M. Davis, and J. Palmer, in *Radar Conference, 2010 IEEE* (IEEE, 2010) pp. 532–537.

[32]C. Moscardini, D. Petri, A. Capria, M. Conti, M. Martorella, and F. Berizzi, IEEE Transactions on Aerospace and Electronic Systems **51**, 1475 (2015).

[33](), `kaira.sgo.fi/2013/09/passive-radar-with-16-dual-coherent.html`.

[34](), `www.rtl-sdr.com/building-a-passive-radar-system-with-an-rtl-sdr`.

[35](2018), `http://superkuh.com/rtlsdr.html`.

[36](), `https://github.com/jmfriedt/gr-oscilloscope`.

[37]D. O'Hagan, H. Griffiths, S. Ummenhofer, and S. Paine, IEEE Transactions on Aerospace and Electronic Systems **53**, 3008 (2017).

[38]Supplementary material.

[39]D. Olivadese, M. Martorella, and F. Berizzi, in *IET International Conference on Radar*

Systems (IET, 2012).

[40]W. Feng, J.-M. Friedt, G. Cherniak, and M. Sato, in *Geoscience and Remote Sensing Symposium (IGARSS), 2018 IEEE International* (IEEE, 2018).